COMMUNICATIONS IN SCIENCE AND TECHNOLOGY
Homepage: cst.kipmi.or.id

Cobalt-nickel supported on desilicated HZSM-5 for the conversion of *Reutealis trisperma* (blanco) airy shaw oil to liquid hydrocarbon products

Lenny Marlinda[a,*], Rahmi[b], Abdul Aziz[b], Achmad Roesyadi[c], Danawati Hari Prajitno[d], Yustia Wulandari Mirzayanti[e], Muhammad Al Muttaqii[f]

[a]*Department of Industrial Chemistry, University of Jambi, Jambi 36361, Indonesia*
[b]*Department of Chemistry, University of Jambi, Jambi 36361, Indonesia*
[c]*Department of Chemical Engineering, Sepuluh Nopember Institute of Technology, Surabaya 60111, Indonesia*
[d]*Department of Industrial Chemical Engineering, Sepuluh Nopember Institute of Technology, Surabaya 60111, Indonesia*
[e]*Adhi Tama Institute of Technology, Department of Chemical Engineering, Surabaya, 60111, Indonesia*
[f]*Research Center for Chemistry-National Research and Innovation Agency, Science and Technology Research Center (PUSPITEK) Area, Tangerang 15310, Indonesia*

Article history:
Received: 20 October 2024 / Received in revised form: 25 May 2025 / Accepted: 25 May 2025

Abstract

Desilication/alkaline treatment and metal impregnation were used to create the HZSM-5 catalyst supported by Co-Ni. These catalysts' isotherm patterns combined type I and type IV isotherms. This isotherm pattern showed a hysteresis loop at comparatively higher pressures. The pore size distribution of the mesoporous HZSM-5 catalysts was situated between 6 and 12 nm in size. Its use in the hydrocracking of *Reutealis trisperma* (Blanco) airy shaw oil (RTO) to produce biofuel was investigated. The results of the catalytic test showed that the hydrocarbon makeup of the biofuel was comparable to that of fuel. In comparison to HZSM-5, the mesoporous Co-Ni/HZSM-5 catalyst enhanced n-paraffin by 46.32 area% and aromatic by 34.18 area% in the hydrocracking of RTO.

Keywords: Desilication; hydrocracking; HZSM-5; liquid hydrocarbon; *Reutealis trisperma* (Blanco) airy shaw

1. Introduction

Biofuels are renewable energy sources that can be produced from plant oils without interfering with food production and provide performance on par with fossil fuels. In view of their high oil content, low extraction costs, adaptability to nutrient-poor soils, and ability to produce by-products such as husks, shells, and cakes that can be turned into organic fertilizers, non-edible vegetable oils like *Cerbera manghas* oil, *Calophyllum inophyllum* oil, *Reutealis trisperma* (Blanco) airy shaw oil (RTO), and Kapok seed oil become all promising options. Additionally, these plants have dense canopies and broad leaves, which enhance their capacity for CO_2 absorption and O_2 production [1-7]. Non-edible oils hold a substantial promise as reliable feedstocks for biodiesel production due to their abundance, cost-efficiency, and high oil yields. Their utilization in biodiesel production mitigates the limitations associated with conventional feedstocks, providing a sustainable alternative [8-9]. These non-edible vegetable oils can be used to produce biofuel, which can limit the use of fossil fuels and alleviate environmental issues by lowering greenhouse gas emissions and increasing the amount of arable land required to maintain energy security and sustainability [9].

Sunan candlenut, or *Reutealis trisperma* (Blanco) airy shaw, is a hardy and versatile plant generally easy to grow and can be harvested once a year after about five years of growth. Dependent upon the species and agroecosystem conditions, an 8-year-old tree is capable of producing 100–150kg of dry seeds, which translates to a crude oil production of roughly 6–8 tons per hectare per year [10]. One of the main byproducts of the oil derived *from Reutealis trisperma* (Blanco) airy shaw seeds is biodiesel, which is a prospective feedstock for the oleochemical, biofuel, and other chemical industries. *Reutealis trisperma* (Blanco) airy shaw biodiesel is noteworthy for having traits that are comparable to those of fossil diesel, which qualifies it for direct use in diesel engines. The oil is poisonous and unfit for human consumption in view of its high concentration of a-elaeostearic acid (51%), palmitic acid (10%), stearic acid (9%), oleic acid (12%), and linoleic acid (19%). As a consequence, it does not compete with food-based biodiesel feedstocks. Its promise as a sustainable bioenergy

* Corresponding author.
Email: marlindalenny@unja.ac.id
https://doi.org/10.21924/cst.10.1.2025.1570

source is confirmed by the fact that its productivity per hectare is on par with that of major biodiesel-producing crops like palm oil [11]. Based on favorable tax and subsidy policies, the estimated life cycle cost of a biodiesel plant using crude RTO is $710 million, with a competitive production cost of $0.69/L and a payback period of 4.34 years [12]. With a maximum yield of 96.53%, the study by Shaah et al. [13] showed that it is feasible to use the non-edible oil from *Reutealis trisperma* (Blanco) airy shaw for biodiesel production through the supercritical methanol technique.

Fatty acids and triglycerides in RTO can be deoxygenated and their carbon chains can be broken by hydrocracking. HZSM-5 is mostly utilized as a catalyst support in the hydrocracking process. It is altered with metal transitions including nickel, cobalt, iron, molybdenum, zinc, or copper to increase the catalyst's activity [1, 4, 14-15]. Every transition metal that is doped into the HZSM-5 catalyst has a distinct function in a cracking process. The production of certain hydrocarbons, such as aromatics or BTXs (benzene, toluene, and xylene), is enhanced by nickel and cobalt modifications in HZSM-5. These dopants have an impact on the catalyst's acidic sites and product selectivity, which ultimately affects the cracking reaction's effectiveness and results [16-18].

In previous research [19–20], the combination of nickel-iron and nickel zinc with HZSM-5 support was prepared for hydrocracking coconut oil to produce biofuel. Theoretically, the changed ZSM-5 pore size affects the metal impregnation process, allowing hydrated metal ions to permeate into the ZSM-5 pore well [21]. Furthermore, it is more possible to enhance the diffusion of hydrocarbon products and triglyceride molecules in a modified ZSM-5 pore compared to the prior state. All of the aforementioned issues are resolved by the presence of the intracrystalline mesopore produced on HZSM-5 through desilication and alkaline treatment [22-23].

The hydrocracking of Sunan Candlenut oil was examined in the work by Al Muttaqii *et al.* [24] to generate aromatic hydrocarbons using a zeolite-based catalyst. When compared to the ZSM-5 catalyst without metal impregnation, the Fe and La metal-impregnated catalyst produced the greatest aromatic component, reaching 35.51%, and improved the acidic sites. Marlinda *et al*. [25] stated that cobalt can regulate nickel's capacity for hydrogenation. The hierarchical Co-Ni/HZSM-5 catalyst's cobalt content increases catalytic activity in the decarboxylation pathway, resulting in the production of pentadecane (n-C_{15}) and heptadecane (n-C_{17}). According to the hierarchical pore structure, the HZSM-5 catalyst has a 15–18% selectivity for monocyclic aromatic hydrocarbons.

To produce the mesoporous HZSM-5 catalyst, a hierarchical pore structure was created in HZSM-5 using desilication. Additionally, to manufacture cobalt-nickel supported on a mesoporous HZSM-5 catalyst, the incipient wetness impregnation approach was selected. Certain apparatus and measurement techniques were used to ascertain the characteristics of catalysts. The hydrocracking of RTO in a pressure batch reactor (model: Paar Company) was then used to observe the catalyst's performance. Here, the impact of Co-Ni metal impregnation and hierarchical pore structure on HZSM-5 and its catalytic characteristics in paraffin (normal/isoparaffin) and aromatic products were then examined.

2. Materials and Methods

2.1. Materials

The RTO was gathered in Indonesia's West Java. Zeolyst International supplied the Ammonium-ZSM-5 zeolite (CBV 8014, 400 m^2/g surface area, 0.05 weight percent Na_2O), which was calcined into HZSM-5 for 5 hours at 550°C. Merck provided the additional compounds, including $Ni(NO_3)_2.6H_2O$ and $Co(NO_3)_2.6H_2O$ with a 98% purity level.

2.2. Preparation and characterization of catalyst

The mesoporous HZSM-5 catalyst was obtained by applying desilication, a common alkaline treatment method and its production process was based on patent IDP000092622. This procedure involved heating 0.2 M NaOH solution to 65°C in a stainless steel vessel, after which HZSM-5 was gradually added to the solution. Zeolite in NaOH solution was then stirred at 200 rpm for 2 hours while being maintained at 65°C. In this experiment, the weight of the HZSM-5 zeolite ratio and the volume of the NaOH solution were 50 cm^3/g. The slurry was then promptly chilled in a water-ice bath, filtered using a vacuum filter, and meticulously cleaned with distilled water until reaching the neutral pH. The removal of sodium ions as the desilication agent from the HZSM-5 crystallites was indicated by the neutral pH. The mesoporous Na-ZSM-5 catalyst was thought to have produced the solids obtained. Furthermore, ion exchange was performed twice using 0.1 M NH_4Cl solution at 80°C to substitute ammonium ions for sodium ions on the mesoporous Na-ZSM-5. The slurry was cleaned and filtered then. After being stored at 60°C for the entire night, the residue—the mesoporous NH_4-ZSM-5—was dried for 12 hours at 120°C. To substitute hydrogen ions for ammonium ions, a mesoporous NH_4-ZSM-5 catalyst was calcined in the air for 5 hours at 550°C. The mesoporous HZSM-5 catalyst is the name given to the solid. A previous study showed that Co-Ni impregnated on different supports (such as HZSM-5 and the mesoporous HZSM-5) was achieved using the incipient wetness impregnation approach [1, 3, 26]. 6 g of catalyst support was gradually wetted with the intended concentration of $Ni(NO_3)_2.6H_2O$ and $Co(NO_3)_2.6H_2O$ aqueous solution while being gently agitated until becoming completely dry. The sample was then reduced with hydrogen at 450°C for 3 hours after being calcined with air for 2 hours at 400°C. The solid mesoporous Co-Ni/HZSM-5 catalyst was obtained by cooling the sample to room temperature using N_2 flow. Table 1 depicts the physical characteristics of catalysts.

2.3. Catalytic hydrocracking tests

With a 600 mL pressure batch reactor (Parr USA 4563) fitted with a mechanical stirrer, the hydrocracking procedure was carried out at hydrogen starting pressure. First, a reactor with 1 g of catalyst was filled with 200 mL of RTO. To eliminate air that had dissolved in the oil or in the reactor twice, the oil was then filtered using nitrogen. The reaction temperature was set at 375°C, and hydrogen was supplied into the reactor. The gas flow was halted when the reactor pressure reached a reaction pressure of 15 to 25 bar. 2 hours passed

during the hydrocracking reaction. Gas chromatography-mass spectrometry and Fourier-transformed infrared spectroscopy were used to examine liquid products. Biofuel was classified as hydrocarbons that resembled gasoline (C_5–C_9), kerosene (C_{10}–C_{13}), and gasoil (C_{14}–C_{22}) [27].

2.4. Characterization of catalyst

X-ray diffraction (XRD, PANanytical X'Pert MPD diffractometer), scanning electron microscopy with energy dispersive X-ray analysis mapping (SEM-EDX, model EVO MA10), and N_2 physisorption in accordance with BET and BJH methods (Quanta-chrome NovaWin Vernsion 11.03 instrument) were used to characterize the Co-Ni/HZSM-5 catalyst.

Furthermore, pyridine adsorption was used to analyze surface acidity. FT-IR spectra of adsorbed pyridine were obtained by means of a Shimadzu IRPrestige-21 FTIR Spectrometer at a resolution of 4 cm^{-1}. Pyridine adsorption was used to analyze a large number of Bronsted acid sites and Lewis acid sites in HZSM-5 changed into meso pore size. 10 milligrams of the sample were put on the sample holder and placed in a Pyrex glass cell with a calcium fluoride (CaF_2) window. In addition, the glass cell was heated for 4 hours at 400°C. After an 1-hour absorption at room temperature, pyridine underwent desorption for 3 hours at 150°C. At room temperature, FTIR spectra in the 1800–1400 cm^{-1} range were observed. Lewis acid sites (L) and Bronsted acid sites (B) were quantitatively analyzed using the absorption of 1450 cm^{-1}, and 1545 cm^{-1}, respectively. Equations 1 and 2 were quantitatively calculated using the Emeis approach, which had also been employed by Wang *et al.* [28].

$$C_{(\text{pyridine on B sites})} = \frac{1.88 \times IA(B) \times R^2}{W} \quad (1)$$

$$C_{(\text{pyridine on L sites})} = \frac{1.42 \times IA(L) \times R^2}{W} \quad (2)$$

where C is the acid side concentration (mmol/g), IA (B or L) indicates the integrated absorbance of the Lewis and Bronsted bands (cm^{-1}); R is the catalyst disk's radius (cm); and W is the disk's weight (mg). Strong Bronsted acid sides were seen in zeolites that already contained transition metals.

The biofuel product was examined using gas chromatography-mass spectrometry (GC-MS, GC: Agilent HP 6890 models 19091S-433, HP-5MS capillary column 30m × 250µm × 0.25µm) and Fourier transformed infrared spectroscopy (FT-IR, Thermo Scientific Nicolet iS10 FTIR).

3. Results and Discussion

3.1. Compositions of Reutealis trisperma (Blanco) airy shaw oil (RTO)

RTO obtained from pressed seeds with a screw press machine consisted primarily of linoleic acid and palmitic acid, i.e. 55.91% and 19.95%, respectively (Table 3). It has been argued that the main polyunsaturated fatty acids are present in RTO [25, 29].

3.2. Characterization of catalyst

3.2.1. Structural and textural properties

Fig. 1 presents the XRD patterns of the catalyst used to hydrocrack RTO. Fig. 1(a) shows the X-ray diffraction pattern of HZSM-5. The MFI framework type of HZSM-5 was shown by the characteristics' peaks at the 2° of 7.87°, 8.74°, 23.04°, 23.24°, 23.64°, 23.91°, and 24.31°. Meanwhile, Fig. 1(b) and (c) demonstrate that the catalysts' XRD patterns matched the distinctive structure of HZSM-5. According to a few former investigations, desiccation and metal impregnation did not alter the crystal structure of HZSM-5 although they caused a drop in the strength of each diffraction peak [16,23,27].

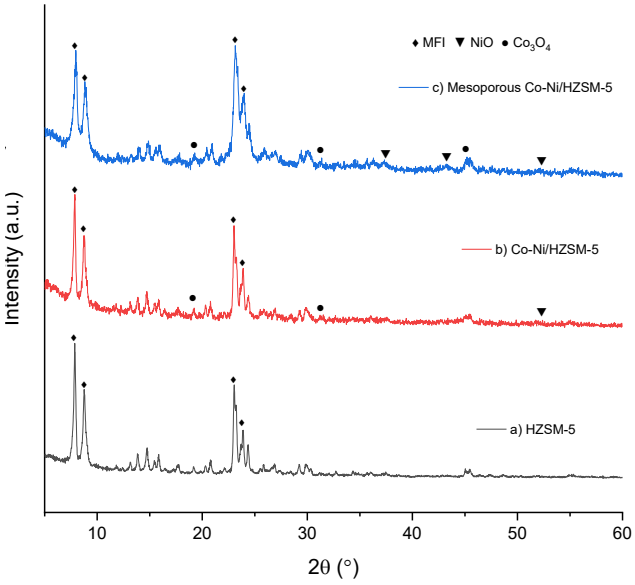

Fig. 1. XRD patterns of catalyst

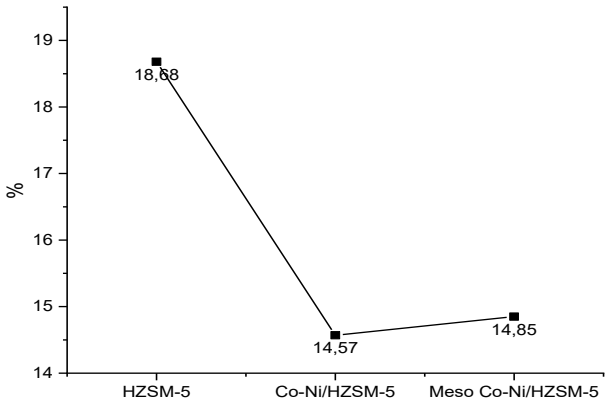

Fig. 2. Crystallinity affected by desilication and metal impregnation

The XRD patterns of the Co-Ni/HZSM-5 catalyst showed the small peak intensity at 2θ of 19.11° and 31.59° for the diffraction of Co_3O_4. As shown in Fig. 1(b), Ni was also detected in the catalyst at 2θ of 52.27°. The most intriguing finding in Fig. 1(c) is that, following calcination and reduction, numerous new phases of Co_3O_4 and NiO species with weak peak intensities were identified in the mesoporous Co-Ni/HZSM-5 catalyst. The inability of the nickel supported on Co/HZSM-5 to fully convert Co_3O_4 and CoO particles into the

metallic phase of Co was most likely the cause of this. Shimura *et al*. and Qin *et al*. [16, 30] stated that nickel supported on Co/HZSM-5 could enhance the Ni Dispersion on HZSM-5 and reduce Co_3O_4 and CoO into cobalt metal due to their reciprocal interactions. Another contributing factor was the hierarchical pore structure of the mesoporous Co-Ni/HZSM-5 catalyst. As a result, obtaining the metallic phase required calcination and a decrease of temperature. Furthermore, as illustrated in Fig. 1(c), Ni metal was found at 37.38° and 43.23° in the Mesoporous Co-Ni/HZSM-5 catalyst with very low intensity. In contrast, as illustrated in Fig. 1(b), no Ni was found at the similar locations for the Co-Ni/HZSM-5 catalyst. This phenomenon was probably related to the incredibly tiny and evenly distributed Ni particles in the zeolite matrix of Co-Ni/HZSM-5, providing weak or undetectable Ni signals in the XRD examination. On the other hand, the mesoporous structure of the Mesoporous Co-Ni/HZSM-5 catalyst promoted the aggregation of Ni metal particles into larger clusters or increased their crystallinity, enabling them to be easier to be identified in XRD examination.

Even though Co was not found in the catalysts, the SEM-EDAX measurement results, as shown in Table 1 and Fig. 3(c), demonstrated the metals' existence. This indicated that the Ni and Co metals were uniformly distributed in extremely insignificant amounts; this was why their XRD peak intensities were either very low or not apparent [17].

However, the desilication and metal impregnation processes on HZSM-5 had an effect on the reduction of its crystallinity (Fig. 2). This was primarily related to the removal of silicon, which could disrupt the structural integrity, causing disorganization within the framework or partial collapse in specific regions [31, 32]. Meanwhile, the decrease in crystallinity resulting from metal impregnation indicated that metal ions was successfully incorporated into the structural framework without any significant disruptions. This reduction is more appropriately attributed to the dispersion of metal particles within the structure rather than an overall decline in crystallinity [33].

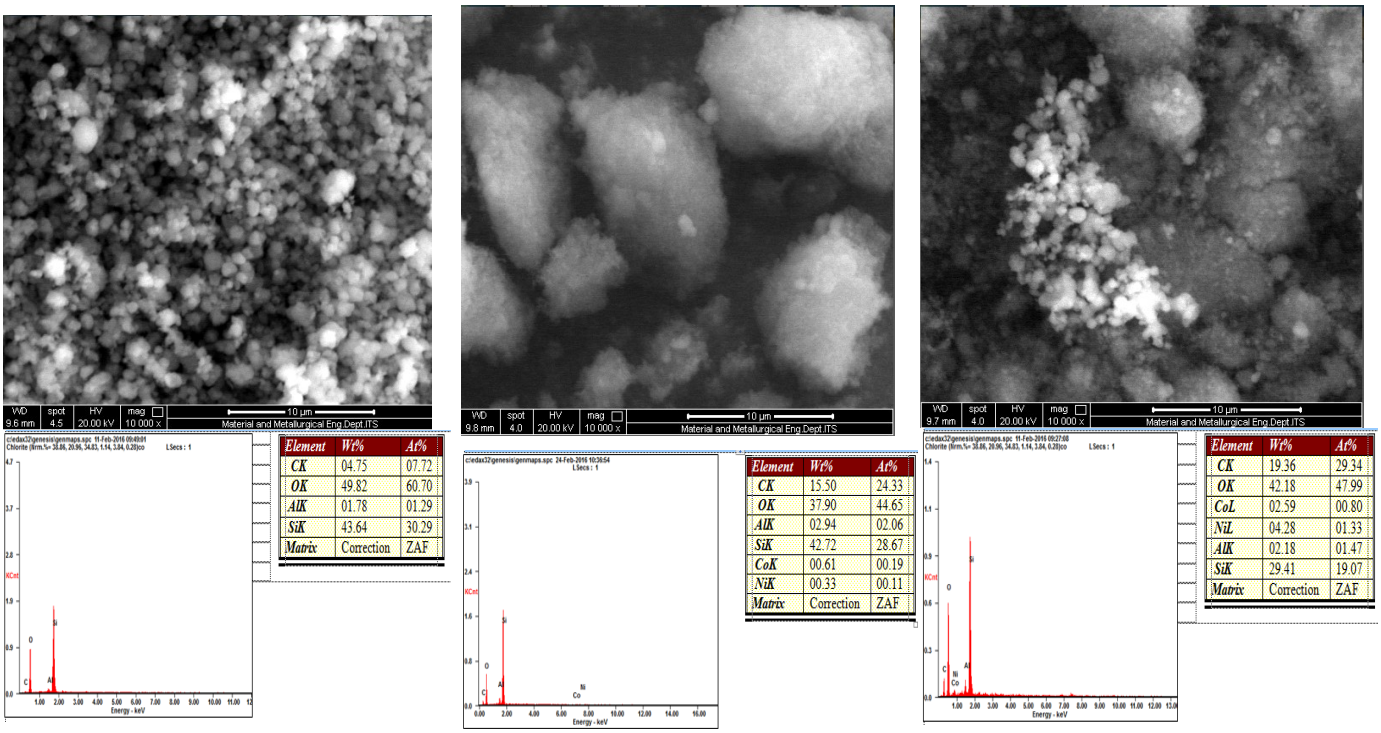

(a) HZSM-5 (b) mesoporous HZSM-5 (c) mesoporous Co-Ni/HZSM-5 after calcined and reduced

Fig. 3. SEM-EDAX image of catalyst.

Table 1. The physical properties of the catalyst.

Catalyst	Surface area, S (m^2/g)			Average pore diameter (nm)	Total pore volume (cm^3/g)	Actual Metal Content[b] (wt.%)	
	S_{BET}	S_{micro}	S_{meso}			Co	Ni
HZSM-5	355.96[a]	303.27	52.69	2.49[a]	0.22[a]	-	-
Mesoporous HZSM-5	447.77	n.d	n.d	10.23	1.15	-	-
Co-Ni/HZSM-5	223.14[a]	189.95	33.19	2.71[a]	0.15[a]	3.55	3.30
Mesoporous Co-Ni/HZSM-5	457.23	n.d	n.d	5.09	1.16	2.59	4.28

[a]be published by Al-Muttaqii *et al.* [1]
[b]EDAX measurement
n.d = not determined

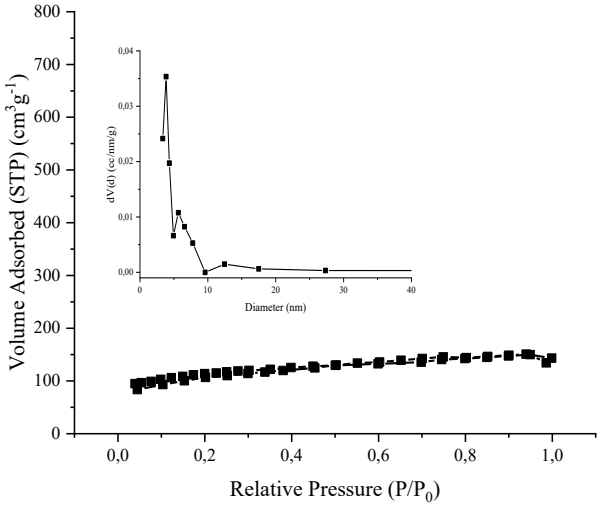

(a). HZSM-5

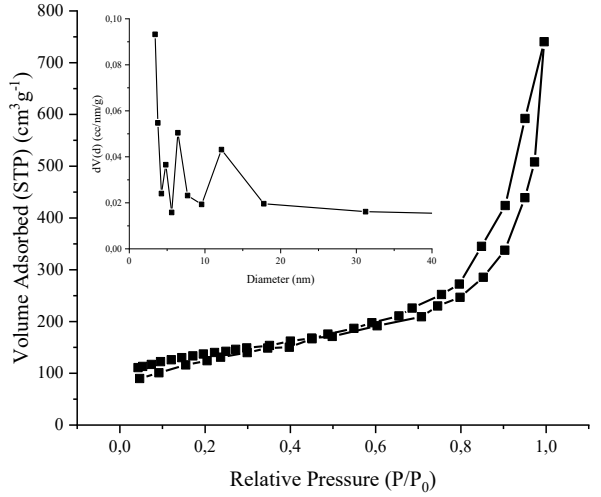

(b). mesoporous HZSM-5 after calcined

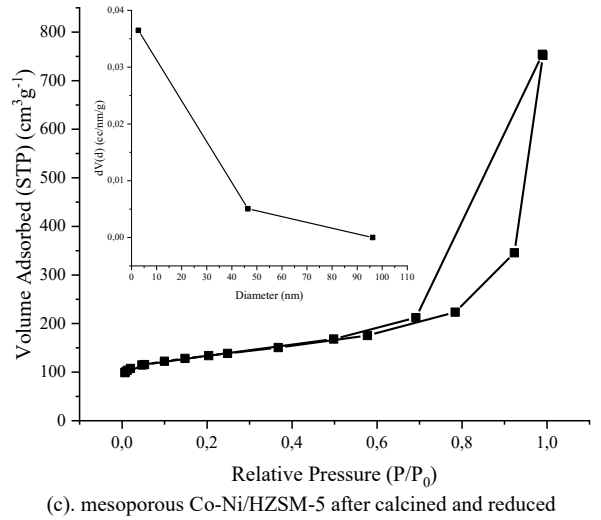

(c). mesoporous Co-Ni/HZSM-5 after calcined and reduced

Fig. 4. Nitrogen isotherms and pore size distribution of catalysts

Fig. 3(b) and 3(c) show the morphology of the catalyst after the desilication process. The catalyst surface defects caused by desilication showed the extraction of Si. In essence, desilication involves selectively removing silicon atoms from the zeolite framework and creating additional porosity. However, in the hydrocracking process, the desilication procedure can increase the catalyst's surface area, mesopore volume, and density, as well as the number of acid sites, catalytic conversion and prolong the catalyst's lifespan [31, 34-35]. It can be proven based on EDAX showing Si/Al ratio dropped from 24.5 wt.% to 14.53 wt.%. Following metal impregnation, the Si/Al ratio dropped from 14.53 wt.% to 13.49 wt.%.

Following desilication on HZSM-5, Table 1 demonstrates that BET surface area and total pore volume significantly increased from 355.96 m^2/g and 0.22 cm^3/g to 447.77 m^2/g and 1.15 cm^3/g, respectively, as reported by Ma *et al*. [36]. These physical properties, however, remained nearly unchanged for the mesoporous Co-Ni/HZSM-5 catalyst following metals impregnation with final surface area and total pore volume by 457.23 m^2/g and 1.16 cm^3/g, respectively. This was most likely caused by Co_3O_4 and NiO particles present in the catalyst's pore and able to provide surface area for themselves, thereby preventing a considerable drop in the overall surface area of catalyst. On this Co-Ni/HZSM-5 catalyst, various phenomena were observed, including a modest decrease in surface area and total pore volume to 223,14 m^2/g and 0.15 cm^3/g, respectively. By obstructing the microporous area and clogging the mesoporous area, the addition of metals resulted in micropore surface area and micropore volume was decreased [17, 21, 37-39].

Fig. 4 illustrates the adsorption pore size distribution and nitrogen isotherms obtained from the BJH technique of a HZSM-5-based catalyst. In accordance to IUPAC's classification of adsorption isotherms, mesoporous HZSM-5 catalyst showed a combined pattern of type I and type IV isotherms, as shown in previous research (Fig. 4(b)) [21-23]. HZSM-5, as illustrated in Fig. 4(a), possessed the type I isotherm of microporous materials. At higher relative pressures, the type IV isotherm verified the existence of a hysteresis loop, which was typified by the development of a hierarchical pore structure on HZSM-5 [21]. Both curves were roughly parallel from P/Po = 0.5 to P/Po = 0.7 since nitrogen desorption did not appear to follow the initial adsorption trend.

The hierarchical pore structure in HZSM-5 enhanced the number of active sites. This was attributed to the introduction of mesopores (larger pores) alongside the intrinsic micropores of HZSM-5, providing a greater surface area for reactant molecules to interact and be adsorbed, ultimately resulting in an increased availability of active sites for catalytic reactions [23]. It can be stated that the hierarchical structure of HZSM-5, characterized by the combination of micro- and mesopores, significantly improved the catalyst's surface area, accessibility, and optimal utilization of active sites. The enlarged surface area directly contributed to a higher number of potential locations for reactants to bind and engage in catalytic processes. In addition to reduce diffusion restrictions that may otherwise impair catalytic activity, the mesopores in the ZSM-5 structure made it simpler for bigger reactant molecules to reach the microporous channels and active sites. This improved accessibility ensures that a greater proportion of active sites can participate in the reaction, thereby enhancing overall catalytic performance. The hierarchical pores allowed for more efficient use of the acidic sites during catalytic reactions by providing access to the active sites inside the ZSM-5 structure. Such a hierarchical architecture is particularly crucial for reactions prone to diffusion limitations due to coke formation, which can significantly reduce catalytic efficiency.

Cobalt and nickel supported on mesoporous HZSM-5 are crucial for generating mesoporosity in the catalyst, which enables the rapid diffusion of big molecules, as shown in Fig. 4(c). Non-uniform pore size can also result from desiccation. Because silicate anions were randomly extracted, leaving a hole in the zeolite structure, the pore size became not uniform. While the micropore size distribution was centered at roughly 0.43 nm and remained nearly constant based on the H-K method, the mesoporosity in the mesoporous HZSM-5 catalyst showed a narrow pore size distribution and a broader pore size distribution centered at 6 nm and 12 nm, respectively, based on the BJH method. Gou *et al.* [22] discovered the same thing, stating that the desilication produced a mesoporous structure in the HZSM-5 crystals while leaving the microporous structure essentially unaltered.

3.2.2. Acidic properties

The FT-IR spectra of adsorbed pyridine (Fig. 5) illustrated how the acidity of HZSM-5 zeolite was determined by alkali treatment and metal addition (Co-Ni). The integrated area (IA) of each characteristic band, as listed in Table 2, was used to determine the number of acid sites. Pyridine was chemically adsorbed on Brønsted and Lewis acid sites, respectively, to form the bands at 1545 and 1445 cm^{-1}. [22].

Separating the impact of HZSM-5's acidic sites from the formation of aromatics was unable to be done. As shown in Table 2, the addition of metals and the desilication process of the hierarchical structure maker of HZSM-5 resulted in Brønsted acid sites (B) fewer and Lewis acid sites more. This phenomenon could be linked to the development of lattice defects and dealumination following treatment with NaOH solution. The aforementioned findings concurred with earlier studies [21-23,31]. Both Lewis and Brønsted acid sites are crucial for catalysis; Lewis acid sites take electron pairs, whereas Brønsted acid sites give protons (H^+). In a variety of processes, the combination of Lewis and Brønsted acid sites can result in an improved catalytic activity. Proton transfer reactions, which are essential for many catalytic processes such as dehydration, isomerization, and cracking reactions, require Brønsted acid sites. The active site of the electron acceptor is represented by the Lewis acid site. However, in a zeolitic catalyst, the Brønsted acid site is an active site that donates protons from the Si(OH)-Al bridge. [40].

The proton on the acid side will be swapped out for the impregnated metal. The creation of carbenium ions, which are intermediate products in the conversion of hydrocarbons that take place in the presence of Brønsted acid (B) and Lewis acid (L) sites, is what determines the selectivity of aromatics and paraffins. It may also be said that both kinds of acids can be enhanced by the Co-Ni-impregnated hierarchical pore-structured support. Figure 9 illustrates how these two acid types contributed to the production of aromatics during the hydrocracking of RTO using a mesoporous Co-Ni/HZSM5 catalyst.

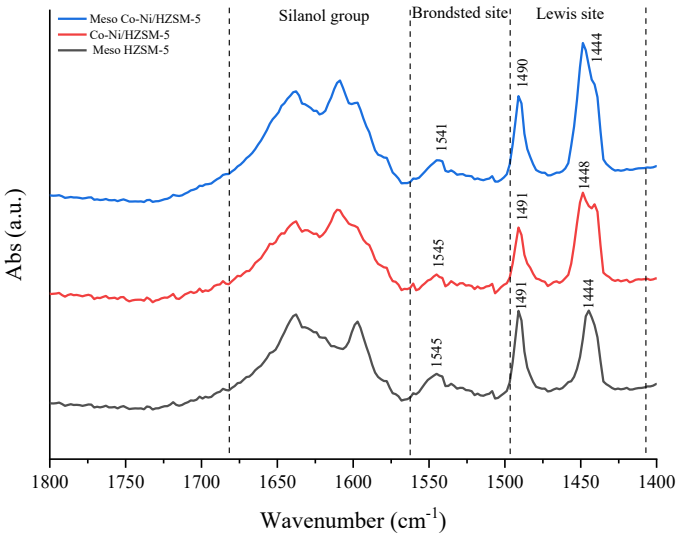

Fig. 5. FT-IR spectra of pyridine adsorption on the parent and alkaline-treated HZSM-5 samples

Table 2. Acidic properties of zeolite

Catalyst	Acid site	Wavenumber range (cm^{-1})	Absorption band (cm^{-1})	Acid area	Lewis acid area (mmol/g)	Brønsted acid site (mmol/g)	Total acidity (mmol/g)	L/B
Meso HZSM-5	L	1431-1462	1445	7.1643	0.35049		0.5254	2.0036
	B	1537-1556	1545	4.7339		0.1749		
Co-Ni/HZSM-5	L	1427-1462	1445	13.3644	0.6716		0.7367	10.3136
	B	1539-1558	1545	1.7155		0.0651		
Meso Co-Ni/HZSM-5	L	1431-1460	1445	17.0567	0.6593		0.7348	8.7336
	B	1531-1562	1545	2.5827		0.0754		

3.3. Analysis of biofuel

As illustrated in Fig. 6(a), the spectra investigation of RTO oil revealed that the carboxylic groups' vibrational modes were intense in the absorption bands at wavenumbers of 1159.66 cm^{-1} and 1741.90 cm^{-1}, corresponding to C−O and C=O bonds, respectively. The RTO analysis results are shown in Fig. 6(a), where carboxyl group vibrations and long-chain fatty acid ester components were observed clearly visible. The prominent peak at 1741.90 cm^{-1} in the 1800–1700 cm^{-1} range was determined to be C=O (ester group). The presence of asymmetric stretching vibration in =C−H bonding and symmetric stretching vibration in $-CH_2$ bonding was confirmed by further peaks at 2921.87 cm^{-1} and 2852.3 cm^{-1}. Peaks at 1238.9, 1159.66, and 1115.39 showed the anti-symmetric vibrations of C−O−C bond [13].

However, as illustrated in Fig. 6(b), the ester of the secondary alcohol band vanished and the FTIR spectra of a liquid product changed to lower frequencies from 1741.90 cm^{-1} to 1707.63 cm^{-1} wavenumbers. As shown in an earlier research [40–43], the anomaly in the FTIR spectra indicated that oxygen was removed from oxygenated compounds to create alkanes during hydrocracking through the

decarboxylation, decarbonylation, and hydrodeoxygenation reaction. The creation of aromatic compounds was indicated by the presence of absorption bands in the FTIR spectra at 722 cm^{-1} and 746 cm^{-1} for liquid products, described as a shift in the shape of the C−H bond.

Figure 7 presents the GC-MS spectra of biofuel and RTO generated at 375°C. The chemicals in the RTO with a retention duration of 10–14 minutes vanished following the reaction, as seen in Fig. 7(a). As the product was retained for 0–12 minutes, the quantity of hydrocarbon compounds in it rose. Table 3 shows that the main components contained in RTO were primarily free fatty acids (such as linoleic acid and palmitic acid) with a minor portion comprising aromatic compounds and alcohols [29].

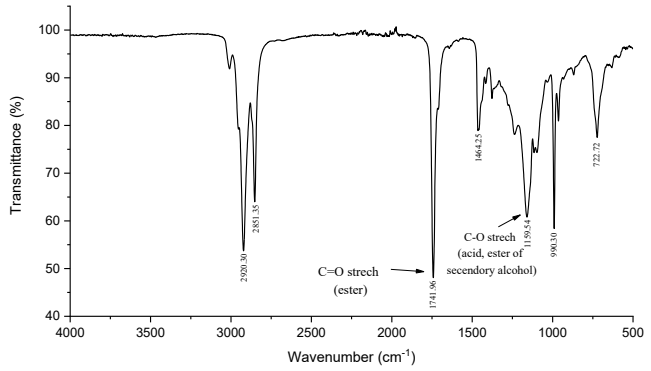

(a) RTO

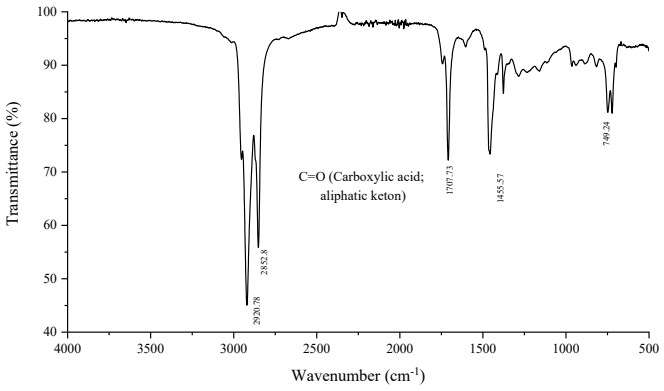

(b) the liquid product obtained at 375°C for 2 hours with Co-Ni/HZSM-5 catalyst

Fig. 6. Spectra FTIR analysis under 20±5 bar in the batch reactor.

As depicted in Fig. 7(b) and Table 4, the monocyclic aromatic hydrocarbons type of aromatic compound that are common in biofuel had chromatograms. N-paraffin, which includes pentadecane (C_{15}) and heptadecane (C_{17}), are the other prevalent compounds.

Fig. 8 shows that the liquid product contained high aromatic hydrocarbons of 47% area for Co-Ni catalyst impregnated on mesoporous HZSM-5. As evidence, the liquid product's n-paraffin content rose due to the mesoporous HZSM-5 catalyst. The carboxylic acid and n-paraffin content of the mesoporous HZSM-5 catalyst both before and after cobalt-nickel metal impregnation showed an intriguing trend. The area of normal paraffin compounds rose from 12% to 34%, while the area of carboxylic acid dropped dramatically from 60% to 2%. Pentadecane made up 18% of the n-paraffin's makeup, whereas heptadecane made up 13%. According to this finding, pentadecane and heptadecane were the most abundant hydrocarbon components in the liquid product. This outcome is nearly identical to what Veriansyah *et al*. [44] reported. It has been demonstrated that mesoporous HZSM-5 with intracrystalline mesoporosity and cobalt-nickel had better intracrystalline diffusion and active sites [23, 39]. The desilication resulted in a reduction of acid sites, consistent with the findings of other research [21, 23, 36]. Additionally, mesoporous HZSM-5's acidity was decreased by the addition of metal. Hao *et al*. [21] reported that, in mesoporous HZSM-5, the metals took the place of the proton. One could argue that HZSM-5's acidity can enhance C-C bond cracking.

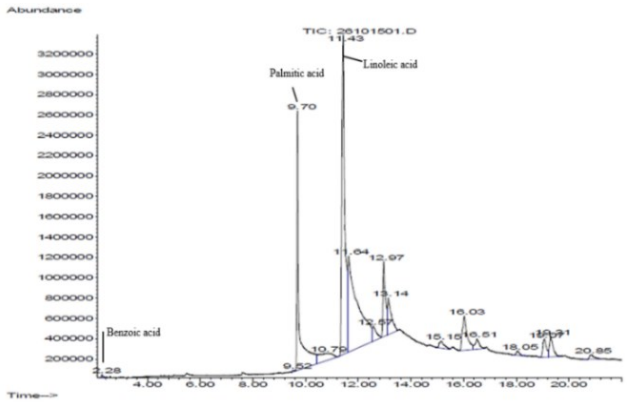

(a) RTO

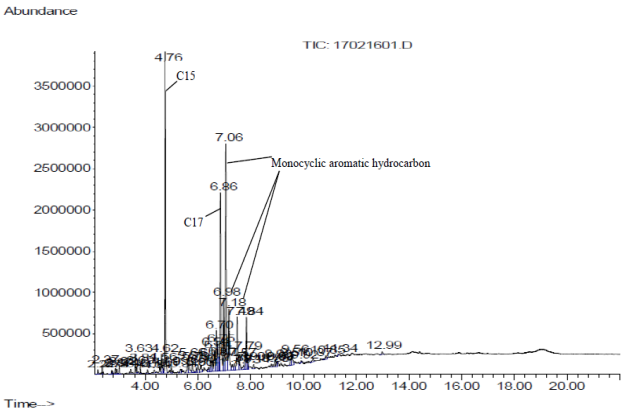

(b) liquid product produced at 375°C for 2 hours with mesoporous Co-Ni/HZSM-5 catalyst

Fig. 7. GC-MS spectra under 20±5 bar in the batch reactor

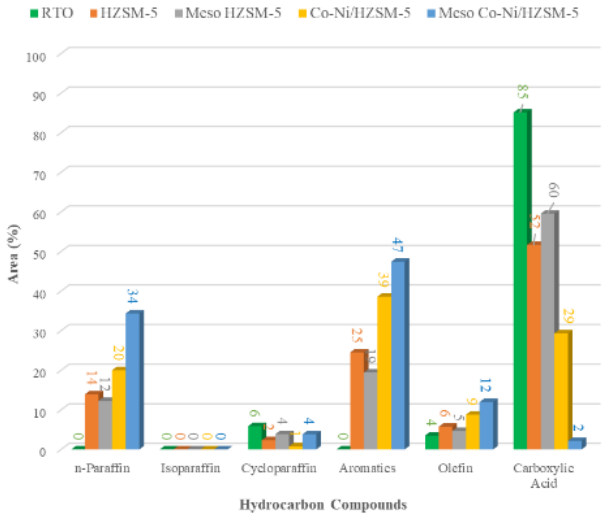

Fig. 8. Effect of hierarchical mesoporous catalyst on hydrocarbon composition in liquid product.

Table 3. Chemical compounds in RTO before catalytic hydrocracking tests

Compound/formula	Structure	RT (min)	Abundance (area%)
n-Hexadecanoic acid (Palmitic acid)/$C_{16}H_{32}O_2$	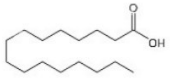	9.70; 10.79	19.95
9,12-Octadecanienoic acid (Linoleic acid)/$C_{18}H_{32}O_2$	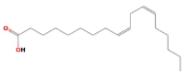	11.43; 11.64	55.91

Table 4. Aromatic compounds in biofuel produced with HZSM-5 based catalyst at 375°C under 20±5 bar in the batch reactor.

Aromatic compound/formula		Structure	RT[a](min)	Abundance (area%)[b]			
				I	II	III	IV
Benzene,-	pentyl-/ $C_{11}H_{16}$	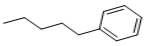	2.32	0	1.28	0.69	0.54
	1-methyl-4-(2-methylpr.../p-Isobutyltoluene / $C_{11}H_{16}$	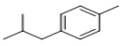	2.37	0.4	4.14	1.46	1.64
	hexyl-/ $C_{12}H_{18}$	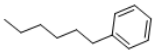	2.87	0.31	1.29	0.56	0.67
	1,3-Dimethylbutylbenzene/ $C_{12}H_{18}$	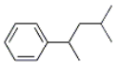	2.93; 7.84	**4.14**	**7.06**	**0.43**	**1.62**
	heptyl-/ $C_{13}H_{20}$	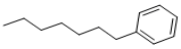	3.63	1.02	1.67	0.75	0.88
	1-Methyl-2-N-Hexylbenzene/$C_{13}H_{20}$	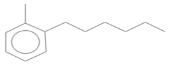	3.69; 5.66	1.59	1.77	0.59	0.7
	(1-methylheptyl)-/2-Phenyloctane/$C_{14}H_{22}$	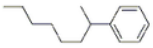	4.09; 4.62	**1.89**	**3.17**	**1.04**	**1.46**
	octyl-/ Phenyloctane/ $C_{14}H_{22}$	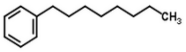	4.56	0.68	1.14	0.57	0.67
	nonyl-/$C_{15}H_{24}$	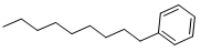	5.61	0.84	1.06	0.59	0.68
	(1-methylnonyl)-/$C_{16}H_{26}$	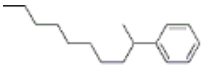	6	0.66	0.79	0	0.58
	1-methyl-4-(1-methylet.../ 4-Isopropyltoluene/ $C_{10}H_{14}$	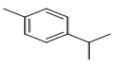	6.12	0.72	0	0	0
	1-methyl-3-(1-methylet…/ 3-isopropyltoluene/ $C_{10}H_{14}$	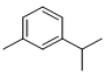	6.41	0.37	0	0	0
	(1-methyldecyl)- /$C_{17}H_{28}$	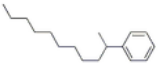	6.98; 7.06;7.18	**26.62**	**12.28**	**5.97**	**4.92**
	-diethyl/$C_{10}H_{14}$		7.18	0	0	1.26	1.47
	1-ethyl-3,5-dimethylbenzene. /5-Ethyl-m-xylene/$C_{10}H_{14}$	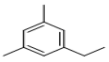	7.49	**4.22**	**2.66**	**0**	**0**
	undecyl-/$C_{17}H_{28}$	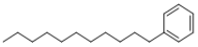	7.58	0	0	1.22	1.42
	tridecyl-/$C_{19}H_{32}$	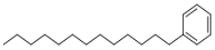	7.79	1.25	0	0	0
	dodecyl-/$C_{18}H_{30}$	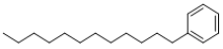	8.85	0.21	0	0	1.37

[a]RT = retention time for Mesoporous Co-Ni/HZSM5 catalyst
[b]I = Mesoporous Co-Ni/HZSM5; II = Co-Ni/HZSM-5; III = Mesoporous HZSM-5; IV = HZSM-5

Table 4 demonstrates that the most of the aromatics generated during hydrocracking were monocyclic aromatic hydrocarbons (MAHs), such as substituted benzenes. The most abundant hydrocarbon component in liquid products for all catalysts was benzoene (1-Methyldecyl). A significant amount of n-$C_{17}H_{36}$ was present, and a significant amount of the equivalent (1-Methyldecyl) benzene was visible. This indicated that the amount of alkylbenzenes generated was proportionate to n-paraffins with the same number of C atoms. Filho *et al.* [45] also reported a similar phenomenon as found in this work. In the case of dodecylbenzene and its isomers, Rabaev *et al.* [44] found that the presence of (1-Methyldecyl) benzene exhibited a migrating process of double bond (conjugated system) along chain fatty acids into carboxylic terminal or methyl group prior to aromatization. There were additional polycyclic aromatic hydrocarbons (PAHs) such butyl and 2-methyl naphthalene. Less than 0.5% of the area had anthracene.

The creation of the substituted benzenes and naphthalenes was enhanced by the combination of metals and the

mesoporous structure. However, the production of PAHs like phenanthrene and anthracene was not aided by impregnation. Additionally, aromatic chemicals generated in the C_5–C_{15} range were identified in gasoline by Vichaphund *et al*. [47]. Consequently, when Co-Ni metals were impregnated into the HZSM-5 pore, 1,3-dimethylbutylbenzene and 1-ethyl-3,5-dimethylbenzene in liquid products were abundant hydrocarbon molecules clustered in gasoline [25]. By raising the octane value, these aromatic chemicals may raise the heating value of biofuel. The liquid substance might also be referred to as biofuel.

The incorporation of Co-Ni metals into hierarchical HZSM-5 has been shown to significantly improve hydrocarbon yields compared to the unmodified catalyst, as demonstrated by Marlinda *et al.* [25]. Furthermore, Rac *et al.* [23] reported that the desilication process not only increased the surface area but also enhanced the distribution of Brønsted acid sites.

As reported by Riyanto *et al*. [48], the addition of Co and Ni metals to HZSM-5 resulted in a greater number of Lewis acid sites as opposed to Brønsted acid sites. When the two metals were successively and independently injected onto the hierarchical zeolite HZSM-5, this was likewise seen. These findings suggest that while desilication of HZSM-5 may result in fewer acid sites, the quantity of acid sites rises once more after the addition of Co-Ni metals. Anggoro *et al*. [49] claimed that the greater number of Lewis acid sites following metal impregnation than Brønsted acid sites was caused by the presence of vacant d-orbitals in transition metals, which were capable of accepting electrons.

The co-impregnation of Co and Mo metals reported by Riyanto *et al*. [48] showed a propensity for a decrease in both Brønsted and Lewis acid sites, as well as total acidity, in contrast to the results observed in our work utilizing the incipient wetness impregnation approach. This drop was ascribed to metal species obstructing the pores, which reduced the surface area and prevented access to acid sites. These results imply that the zeolite's acidity is greatly determined by the impregnation technique.

As shown in Table 2, the catalyst generated in this investigation was shown to have a low Brønsted-to-Lewis (B/L) acid site ratio. In Fig. 9, the combination of these two kinds of acid sites encouraged the synthesis of aromatic molecules. Additionally, the C_{15}/C_{16} ratio showed that the decarboxylation reaction, controlling the RTO hydrocracking process, was efficiently promoted by all catalysts; as a consequence, this helped to lower the amount of hydrogen used.

The function of Lewis and Bronsted acid sites in the synthesis of aromatic and paraffin compounds is illustrated in Fig. 9. Chen *et al*. [50] stated that the process of fatty acid deoxygenation is the first step in the reaction mechanism of aromatic synthesis. This process yields paraffin compounds (alkanes) by following the general pathway of hydrocracking reactions (decarboxylation/decarbonylation and hydrodeoxygenation). At the Bronsted acid site, alkane compounds with an atomic chain length of C_{15}–C_{18} hydrocracked into alkanes (C_2-C_{10}), while some cracked into alkenes (C_2-C_{10}). Lewis acid sites and olefins enabled cyclization processes to produce intermediates, subsequently dehydrogenated at the Brounsted acid site to produce aromatic compounds. Additionally, these intermediates were hydrogenated to create cyclic molecules.

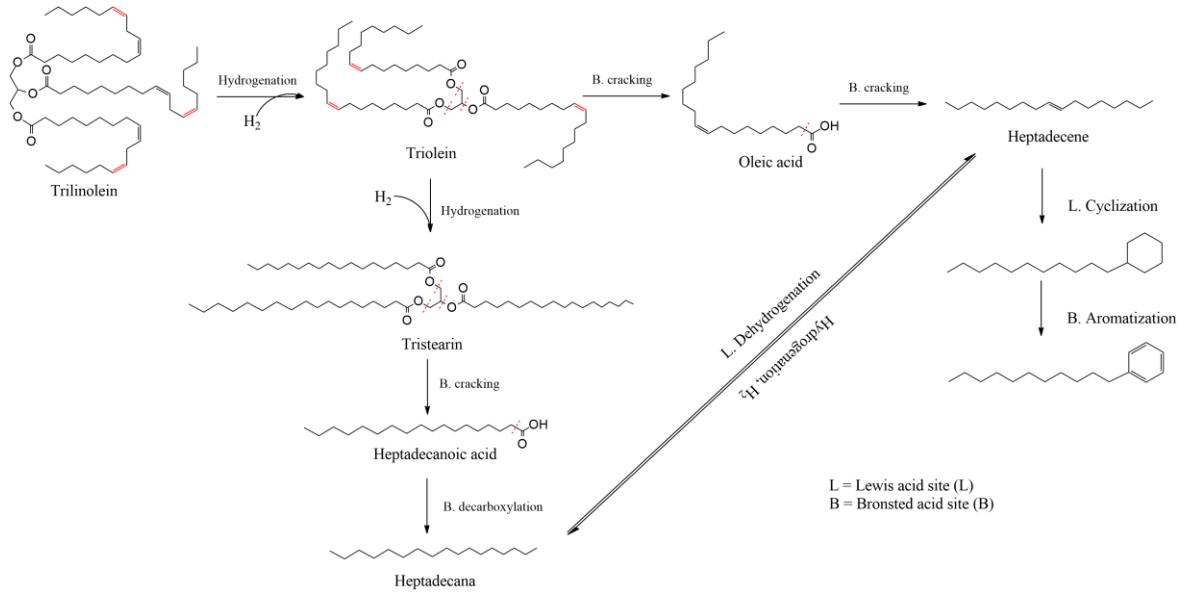

Fig. 9. Prediction of the mechanism of aromatic formation from hydrocracking of RTO with Co-Ni/HZSM-5 meso catalyst at a temperature of 375°C

4. Conclusion

Through desilication, a mesoporous HZSM-5 catalyst was produced. The meso-microporous hierarchical pore structure of this catalyst was able to decrease the diffusion routes of triglyceride molecules and enhanced the number of active sites. Co-Ni impregnation on mesoporous HZSM-5 could also enhance the textural characteristics of catalysts. It has been demonstrated that the combination of desilication and Co-Ni impregnation increased the quantity of hydrocarbon compounds, such as n-paraffins, isoparaffins, cycloparaffins, and aromatics, in the hydrocracking of RTO. The mesoporous Co-Ni/HZSM-5 catalyst exhibited an aromatic area of 46.32% and an n-paraffin area of 34.18%.

Acknowledgements

DP2M-DIKTI, LPPM Skema Penelitian Terapan Universitas Jambi (No.306/UN21.11/PT.01.05/SPK/2024), RIIM LPDP Grant, and BRIN (National Research and Innovation Agency) with grant numbers B-844/II.7/FR.06/5/2023 and B-948/III.10/FR.06/5/2023 are all acknowledged by the authors for their research grants. We are grateful to the laboratory crews, Muhammad Rizki Indra Saputra and Akhmad Ridho, as well as the Head of Chemical Reaction Engineering Laboratory, Department of Chemical Engineering, Faculty of Industrial Technology, Sepuluh Nopember Institute of Technology, for the facilities.

References

1. M. Al-Muttaqii, L. Marlinda, A. Roesyadi, and D. Hari Prajitno, *Co-Ni/HZSM-5 Catalyst for Hydrocracking of Sunan Candlenut Oil (Reutealis trisperma (Blanco) Airy Shaw) for Production of Biofuel*, The J. pure appl. chem. res. 6 (2017) 84–92.
2. L. Marlinda, M. Al-Muttaqii, A. Roesyadi, and D. H. Prajitno, *Formation of hydrocarbon compounds during the hydrocracking of non-edible vegetable oils with cobalt-nickel supported on hierarchical HZSM-5 catalyst*, *IOP Conference Series: Earth and Environmental Science, Institute of Physics Publishing*, 2017.
3. L. Marlinda, M. Al Muttaqii, and A. Roesyadi, *Production of Biofuel by Hydrocracking of Cerbera Manghas Oil Using Co-Ni/HZSM-5 Catalyst: Effect of Reaction Temperature*, The J. pure appl. chem. res. 5 (2016) 189–195.
4. Y. W. Mirzayanti, A. Roesyadi, and D. H. Prajitno, *Triglyceride of Kapok seed Oil to biofuel over a synthesised Cu-Mo supported HZSM-5 catalyst, IOP Conference Series: Materials Science and Engineering, Institute of Physics Publishing,* 2019.
5. D. H. Prajitno, A. Roesyadi, M. Al-Muttaqii, and L. Marlinda, *Hydrocracking of non-edible vegetable oils with Co-Ni/HZSM-5 catalyst to gasoil containing aromatics*, Bull. Chem. React. Eng. Catal. 12 (2017) 318–328.
6. R. Rasyid, A. Prihartantyo, M. Mahfud, and A. Roesyadi, *Hydrocracking of Calophyllum inophyllum oil with non-sulfide CoMo catalysts*, Bull. Chem. React. Eng. Catal. 10 (2015) 61–69.
7. E. G. S. Junior, L. F. B. D. Souza, V. H. Perez, F. D. S. Melo, N. F. D. Santos *et al.*, *Non-edible Oil Plants for Biodiesel Production*, in *Clean Energy Production Technologies: Novel Feedstocks for Biofuels Production*, A. Guldhe and B. Singh, Eds., Singapore: Springer, 2022.
8. M. A. H. Shaah, F. Allafi, M. S. Hossain, A. Alsaedi, N. Ismail, M. O. A. Kadir *et al., Candlenut oil: review on oil properties and future liquid biofuel prospects*, Renew Sust Energ Rev. 45 (2021) 17057–17079.
9. M. A. H. Shaah, M. S. Hossain, F. A. S. Allafi, A. Alsaedi, N. Ismail, M. O. A. Kadir *et al.*, *A review on non-edible oil as a potential feedstock for biodiesel: physicochemical properties and production technologies*, RSC Adv. 11 (2021) 25018–25037.
10. M. Herman, B. Hafif, Y. Ferry and A. Aunillah, *The prospect of kemiri sunan (Reutalis trisperma B. airy shaw) development as a source of bio-oil from inedible crops, E3S Web of Conferences, EDP Sciences,* 2023.
11. S. Supriyadi, P. Purwanto, H. Hermawan, D. D. Anggoro, C. Carsoni, and A. Mukhtar, *Characteristics of Kemiri Sunan (reutalis trisperma (blanco) airy shaw) biodiesel processed by a one stage transesterification process*, *IOP Conference Series: Earth and Environmental Science, IOP Publishing Ltd,* 2021.
12. T. M. I. Riayatsyah, H. C. Ong, W. T. Chong, L. Aditya, H. Hermansyah, and T. M. I. Mahlia, *Life cycle cost and sensitivity analysis of reutealis trisperma as non-edible feedstock for future biodiesel production*, Energies (Basel), 10 (2017).
13. M. A. H. Shaah, M. S. Hossain, F. Allafi, M. O. Ab Kadir, and M. I. Ahmad, *Biodiesel production from candlenut oil using a non-catalytic supercritical methanol transesterification process: optimization, kinetics, and thermodynamic studies*, RSC Adv. 12 (2022) 9845–9861.
14. M. Al-Muttaqii, F. Kurniawansyah, D. H. Prajitno, and A. Roesyadi, *Hydrocracking process of coconut oil using Ni-Zn/HZSM-5 catalyst for hydrocarbon biofuel production*, *Journal of Physics: Conference Series, IOP Publishing Ltd*, 2021.
15. Y. W. Mirzayanti, F. Kurniawansyah, D. Hari Prajitno, and A. Roesyadi, *Zn-Mo/HZSM-5 Catalyst for Gasoil Range Hydrocarbon Production by Catalytic Hydrocracking of Ceiba pentandra Oil'*, Bull. Chem. React. Eng. Catal. 13 (2018) 136–143.
16. L. Qin, J. Li, S. Zhang, Z. Liu, S. Li, and L. Luo, *Catalytic performance of Ni-Co/HZSM-5 catalysts for aromatic compound promotion in simulated bio-oil upgrading*, RSC Adv, 13 (2023) 7694–7702.
17. I. M. S. Anekwe, B. Oboirien, and Y. M. Isa, *Catalytic conversion of bioethanol over cobalt and nickel-doped HZSM-5 zeolite catalysts,* Biofuels, Bioprod. Bioref. 8 (2024) 686–700.
18. I. M. S. Anekwe, B. Oboirien, and Y. M. Isa, *Performance evaluation of a newly developed transition metal-doped HZSM-5 zeolite catalyst for single-step conversion of C1-C3 alcohols to fuel-range hydrocarbons*, Energy Adv. 3 (2024) 1314–1328.
19. M. Al-Muttaqii, F. Kurniawansyah, D. H. Prajitno, and A. Roesyadi, *Hydrocracking of coconut oil over Ni-Fe/HZSM-5 catalyst to produce hydrocarbon biofuel*, Indones. J. Chem. 19 (2019) 319–327.
20. M. Al-Muttaqii, F. Kurniawansyah, D. H. Prajitno, and A. Roesyadi, *Bio-kerosene and bio-gasoil from coconut oils via hydrocracking process over Ni-Fe/HZSM-5 catalyst*, Bull. Chem. React. Eng. Catal., 14 (2019) 309–319.
21. K. Hao, B. Shen, Y. Wang, and J. Ren, *Influence of combined alkaline treatment and Fe-Ti-loading modification on ZSM-5 zeolite and its catalytic performance in light olefin production*, J. Indust. Eng. Chem. 18 (2012) 1736–1740.
22. M. L. Gou, R. Wang, Q. Qiao, and X. Yang, *Effect of mesoporosity by desilication on acidity and performance of HZSM-5 in the isomerization of styrene oxide to phenylacetaldehyde*, Microporous and Mesoporous Materials, 206 (2016) 170–176.
23. V. Rac, V. Rakíc, Z. Miladinovíc, D. Stošić, and A. Aurouxc, *Influence of the desilication process on the acidity of HZSM-5 zeolite*, Thermochim Acta, 567 (2013) 73–78.
24. M. Al-Muttaqii, M. P. Marbun, S. Sudibyo, A. Aunillah, D. Pranowo, H. Hasanudin *et al*., Conversion of Sunan Candlenut Oil to Aromatic Hydrocarbons with Hydrocracking Process Over Nano-HZSM-5 Catalyst, Bull. Chem. React. Eng. Catal, 19 (2024) 141–148.
25. L. Marlinda, M. Al-Muttaqii, A. Roesyadi, and D. H. Prajitno, *Effect of cobalt supported on the hierarchical Ni/HZSM-5 catalyst in hydrocracking of Sunan candlenut oil (Reutealis trisperma (Blanco) airy shaw)*, *Journal of Physics: Conference Series, Institute of Physics Publishing,* 2020.
26. L. Marlinda, M. Al-Muttaqii, I. Gunardi, A. Roesyadi, and D. H. Prajitno, *Hydrocracking of Cerbera manghas Oil with Co-Ni/HZSM-5 as Double Promoted Catalyst*, Bull. Chem. React. Eng. Catal. 12 (2017) 167–184.
27. A. E. Barrón, J. A. Melo-banda, J. M. Dominguez, E. Hernandez, R. Silva, A. I. Reyes *et al*., *Catalytic hydrocracking of vegetable oil for agrofuels production using Ni-Mo, Ni-W, Pt and TFA catalysts supported on SBA-15*, Catal. Today, 116 (2011) 102–110.

28. C. Wang, Q. Liu, J. Song, W. Li, P. Li, R. Xu *et al*., *High quality diesel-range alkanes production via a single-step hydrotreatment of vegetable oil over Ni/zeolite catalyst*, Catal Today, 234 (2014) 153–160.
29. H. Juwono, A. Zakiyah, R. Subagyo, and Y. Kusumawati, *Facile Production of Biodiesel from Candlenut Oil (Aleurites moluccana L.) Using Photocatalytic Method by Nano Sized-ZnO Photocatalytic Agent Synthesized via Polyol Method*, Indones. J. Chem. 23 (2023) 1304–1314.
30. K. Shimura, T. Miyazawa, T. Hanaoka, and S. Hirata, *Fischer-Tropsch synthesis over alumina supported bimetallic Co-Ni catalyst: Effect of impregnation sequence and solution*, J. Mol. Catal. A Chem. 407 (2015) 15–24.
31. L. S. Da Silva, C. A. Araki, S. M. P. Marcucci, V. L. D S. T. D. Silva, and P. A. Arroyo, *Desilication of ZSM-5 and ZSM-12 Zeolites with Different Crystal Sizes: Effect on Acidity and Mesoporous Initiation*, Materials Research. 22 (2019) 1–9.
32. F. Gorzin, J. Towfighi Darian, F. Yaripour, and S. M. Mousavi, *Preparation of hierarchical HZSM-5 zeolites with combined desilication with NaAlO 2 /tetrapropylammonium hydroxide and acid modification for converting methanol to propylene*, RSC Adv. 8 (2018) 41131–41142.
33. H. Heriyanto, O. Muraza, G. A. Nasser, M. A. Sanhoob, I. A. Bakare, Budhijanto *et al*., *Improvement of Catalyst Activity in Methanol-to-Olefin Conversion via Metal (Sr/La) Impregnation over ZSM-5 Catalyst*, Int. J. Technol. 14 (2023) 142–151.
34. D. Dittmann, E. Kaya, and M. Dyballa, *Desilicated ZSM-5 Catalysts: Properties and Ethanol to Aromatics (ETA) Performance*, ChemCatChem. 15 (2023) 1–12.
35. Y. Hou, X. Li, M. Sun, C. Li, S. H. Bakhtiar, K. Lei *et al*., *The effect of hierarchical single-crystal ZSM-5 zeolites with different Si/Al ratios on its pore structure and catalytic performance*, Front. Chem. Sci. Eng. 15 (2021) 269–278.
36. Q. Ma, T. Fu, Y. Wang, H. Li, L. Cui, and Z. Li, *Development of mesoporous ZSM-5 zeolite with microporosity preservation through induced desilication*, J. Mater. Sci. 55 (2020) 11870–11890.
37. S. Wang, Q. Yin, J. Guo, B. Ru, and L. Zhu, *Improved Fischer-Tropsch synthesis for gasoline over Ru, Ni promoted Co/HZSM-5 catalysts*, Fuel, 8 (2013) 597–603.
38. A. N. Aini, M. Al-Muttaqii, A. Roesyadi, and F. Kurniawansyah, *Performance of Ni-Cu/HZSM-5 catalyst in hydrocracking process to produce biofuel from cerbera manghas oil*, *Key Engineering Materials, Trans Tech Publications Ltd*, 2021, pp. 149–156.
39. E. D. da S. Ferracine, K. T. G. Carvalho, D. S. A. Silva, and E. A. Urquieta-Gonzalez, *Carbon-Templated Mesopores in HZSM-5 Zeolites: Effect on Cyclohexane Cracking*, Catal Letters. 150 (2020) 3481–3494.
40. S. S. Vieira, Z. M. Magriotis, M. F. Ribeiro, I. Graca, A. Fernandes, J. M. F. M. Lopes *et al*., *Use of HZSM-5 modified with citric acid as acid heterogeneous catalyst for biodiesel production via esterification of oleic acid*, Microporous and Mesoporous Mater. 201 (2015) 160–168.
41. I. Barroso-Martín, D. Ballesteros-Plata, A. Infantes-Molina, M. O. Guerrero-Pérez, J. Santamaría-González, and E. Rodríguez-Castellón, *An Overview of Catalysts for the Hydrodeoxygenation Reaction of Model Compounds from Lignocellulosic Biomass'*, IET Renew. Power Gener. 16 (2022) 3009–3022.
42. J. García-Dávila, E. Ocaranza-Sánchez, M. Rojas-López, J. A. Muñoz-Arroyo, J. Ramírez, and A. L. Martínez-Ayala, *Jatropha curcas L. oil hydroconversion over hydrodesulfurization catalysts for biofuel production*, Fuel. 135 (2014) 380–386.
43. M. Romero, A. Pizzi, G. Toscano, A. A. Casazza, G. Busca, B. Bosio *et al*., *Preliminary experimental study on biofuel production by deoxygenation of Jatropha oil*, Fuel Process. Technol. 137 (2015) 31–37.
44. B. Veriansyah, J. Y. Han, S. K. Kim, S. Hong, Y. J. Kim, J. S. Lim *et al*., *Production of renewable diesel by hydroprocessing of soybean oil: Effect of catalysts*, Fuel. 94 (2012) 578–585.
45. G. N. da R. Filho, D. Brodzki, and G. Djega-Mariadassou, *Formation of alkanes, alkylcycloalkanes and alkylbenzenes during the catalytic hydrocracking of vegetable oils*, Fuel. 72 (1993) 543–549.
46. M. Rabaev, M. V. Landau, R. Vidruk-Nehemya, V. Koukouliev, R. Zarchin, and M. Herskowitz, *Conversion of vegetable oils on Pt/Al2O3/SAPO-11 to diesel and jet fuels containing aromatics*, Fuel. 161 (2015) 287–294.
47. S. Vichaphund, D. Aht-Ong, V. Sricharoenchaikul, and D. Atong, *Production of aromatic compounds from catalytic fast pyrolysis of Jatropha residues using metal/HZSM-5 prepared by ion-exchange and impregnation methods*, Renew. Energy. 79 (2015) 28–37.
48. T. Riyanto, I. Istadi, B. Jongsomjit, D. D. Anggoro, A. A. Pratama, and M. A. Al Faris, *Improved brønsted to lewis (B/L) ratio of co-and mo-impregnated ZSM-5 catalysts for palm oil conversion to hydrocarbon-rich biofuels*, Catalysts. 11 (2021).
49. D. D. Anggoro, L. Buchori, G. C. Silaen, and R. N. Utami, *Preparation, characterization, and activation of Co-Mo/Y zeolite catalyst for coal tar conversion to liquid fuel*, Bull. Chem. React. Eng. Catal. 12 (2017) 219–226.
50. H. Chen, Q. Wang, X. Zhang, and L. Wang, *Quantitative conversion of triglycerides to hydrocarbons over hierarchical ZSM-5 catalyst*, Appl. Catal. B. (2015) 166–167.